# Enhanced π-π stacking between dipole-bearing single molecules revealed by conductance measurement

Chengyang Zhang[1,#], Jie Cheng[2,#], Qingqing Wu[3,#], Songjun Hou[3], Sai Feng[1], Bo Jiang[4], Colin J. Lambert[3,*], Xike Gao[2,*], Yueqi Li[1,*] and Jinghong Li[1,5,*]

[1]Center for Bioanalytical Chemistry, University of Science and Technology of China, Hefei 230026, China

[2]Key Laboratory of Synthetic and Self-Assembly Chemistry for Organic Functional Molecules, Shanghai Institute of Organic Chemistry, University of Chinese Academy of Sciences, Chinese Academy of Sciences, Shanghai 200032, China

[3]Department of Physics, Lancaster University, Lancaster LA1 4YB, UK.

[4]State Key Laboratory of Analytical Chemistry for Life Science, School of Chemistry and Chemical Engineering, Nanjing University, Nanjing 210023, China

[5]Department of Chemistry, Key Lab of Bioorganic Phosphorus Chemistry and Chemical Biology, Tsinghua University, Beijing 100084, China

*This manuscript is dedicated to the memory of Professor Nongjian Tao.*

**ABSTRACT:** Dipoles are widely involved in π-π interactions and are central to many chemical and biological functions, but their influence on the strength of π-π interactions remains unclear. Here we report a study of π-π interaction between azulene-based, polar single molecules and between naphthalene based, nonpolar single molecules. By performing scanning tunneling microscopy break junction (STM-BJ) measurements of single-molecule conductance, we show that the π-stacked dimers formed by the azulene-based, polar aromatic structures feature higher electrical conductivity and mechanical stability than those formed from the naphthalene-based, nonpolar molecules. Mechanical control of π-π interactions in both rotational and translational motion reveals a sensitive dependence of the stacking strength on relative alignment between the dipoles. The antiparallel alignment of the dipoles was found to be the optimal stacking configuration that underpins the observed enhancement of π-π stacking between azulene-based single molecules. DFT calculations further explained the observed enhancement of stacking strength and the corresponding charge transport efficiency. Our experimental and theoretical results show that the antiparallel alignment of the dipole moments significantly enhances the electronic coupling and mechanical stability of π-π stacking. In addition, in the formation of single-molecule junctions, the azulene group was experimentally and theoretically proved to form an Au-π contact with electrodes with high charge transport efficiency. This paper provides evidence and interpretation of the role of dipoles in π-π interactions at single-molecule level, and offers new insights into potential applications in supramolecular devices.

## Introduction

π-π stacking, as an archetypal form of non-covalent interactions between aromatic structures, has been explored in a wide range of contexts, including supramolecular chemistry [1], material science [2], chemical sensing [3, 4] and molecular biology [5]. With the development of advanced techniques for detecting weak interactions, increasing interest has been focused on the measurement, interpretation and application of π-π stacking. At a macroscopic level, UV-Vis spectroscopy is capable of detecting the existence of π-π stacking [6] and X-ray crystallography can be used to analyze the relative alignment of aromatic rings in crystal structures [7]. However, because the strength and configuration of stacking in the bulk are influenced by multiple types of intermolecular forces from a large number of surrounding molecules, it is difficult to disentangle the contribution from π-π interactions. The emergence of single-molecule measurement techniques, such as force spectroscopy [8], single-molecule fluorescence [9] and break junction conductance measurement [10-12], offers new strategies for characterizing π-π interactions between two single molecules. In particular, break junction conductance measurements of the electrical and mechanical properties of molecular junctions, are a powerful method for studying π-π interactions between single molecules [10-12], due to their

influence on the electronic coupling between neighboring aromatic groups.

Dipoles are commonly involved in the π-π interactions between building blocks of supramolecular assemblies [13] or nucleobases in DNA [14]. A relation between molecular dipoles and stacking properties was also proposed by theoretical considerations [15]. Therefore, investigating the role of dipoles as a contribution to π-π interactions is essential for the interpretation of relevant chemical or biological processes and the design of functional materials or supramolecular systems. Recent X-ray crystallography studies reveal regular alignment of dipoles in crystal structures formed via π-π interactions [7, 16]. However, since crystal formation is a cooperative phenomenon mediated by a large population of molecules, evaluation of the influence from individual dipoles on π-π stacking remains a difficult task. Even at a single-molecule level, because the involvement of dipoles increases the complexity of deciphering the weak, intermolecular interactions, observation and interpretation of dipolar contributions to π-π interactions are still a challenge.

Here we show via single-molecule conductance measurements and mechanical control that the antiparallel alignment of dipole moments significantly enhances π-π interactions between azulene-based molecules, and the enhancement is sensitive to the dipole orientation. We investigated the electronic coupling and mechanical stability of π-π stacking between polar azulene-based single molecules (with a 1.08 D dipole moment [17]) and between non-polar naphthalene-based single molecules. We further determined how the stacking properties were influenced by relative orientation of the dipole moments. Our theoretical modeling confirmed that the optimal antiparallel alignment of the dipoles strengthens the π-π interaction and the corresponding charge transport efficiency. Furthermore, our comparison between the structures terminated with mono-SMe and two-SMe revealed efficient coupling of azulene to an electrode, and also showed different π-π stacking strength due to the steric hindrance introduced by the additional -SMe group. This work provides single-molecule-level evidence that the orientation and strength of π-π stacking are closely related to the dipoles in aromatic groups, and point to new understanding and applications of dipole-mediated π-π interactions.

## Results and Discussions

### Experimental design

To study the effect of dipoles on π-π interactions, we performed scanning tunneling microscopy break junction (STM-BJ) measurements [18-20] of the electrical conductivity and mechanical stability of the π-π stacking between single molecules with and without intrinsic dipoles. The STM-BJ technique measures the conductance of the metal-molecule-metal junctions formed during the piezo-controlled repeated approaching and retraction of the STM tip electrode relative to the substrate electrode (**Experimental section, Fig. 1a**). The measurement provides detailed information under precise mechanical control of the electronic coupling of the molecular junction, and has proved to be sensitive enough to detect the intermolecular coupling between single molecules [11, 21]. We measured the conductance and mechanical stability of a series of azulene-based compounds (AZ1, AZ2 and AZ3) and an isomeric, naphthalene-based compound (NA1). **Fig. 1b** shows the molecular structures and the **Experimental section** describes the synthesis and characterization of these compounds. The compounds are functionalized with methylthio terminal groups to form robust mechanical and electrical contacts with the STM Au electrode on one end (AZ1, AZ3 and NA1) or both ends (AZ2) [22, 23]. Apart from single-molecule junctions, π-stacked dimer junctions (**Fig. 1a**) are also expected to constitute part of the population in break-junction measurements [10, 11, 24], especially for the molecules containing a single anchor group. We investigated the effect of dipoles on π-π interactions by comparing the electrical and mechanical properties of the stacked dimers with polar (azulene) or nonpolar (naphthalene) aromatic groups. In particular, azulene has a 1.08 D dipole moment along an axis from its seven-membered ring to five-membered ring, as a result of the intra-molecular electron transfer to maintain its aromatic structure [25, 26]. The different substitution positions on the phenyl rings (para for AZ1 vs. meta for AZ3) provide an opportunity for accessing different directions of mechanical intervention with respect to the dipole moments.

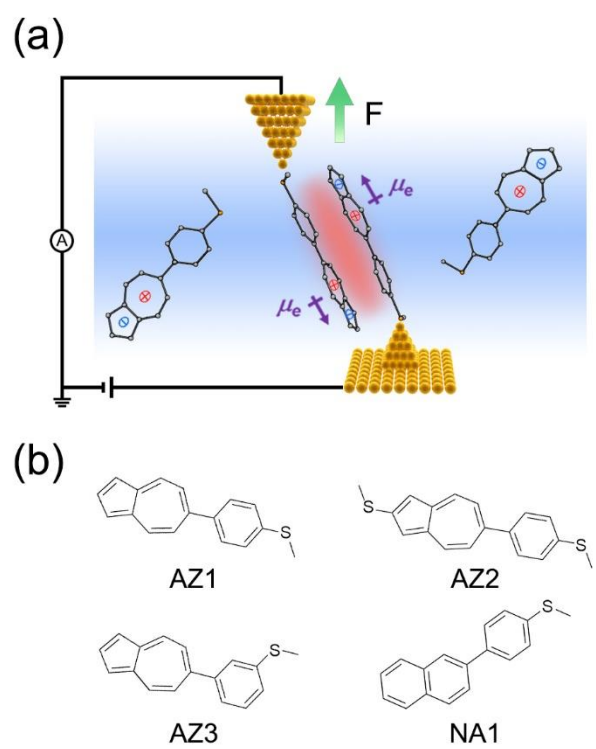

**Figure 1. Schematic diagram of the instrument and chemical structures of the studied compounds. (a)** A scheme of two π-π stacked molecules bridged between the STM electrodes. **(b)** Chemical structures of the studied compounds.

## Conductance measurements reveal π-π stacking between single molecules

We first carried out STM-BJ conductance measurements for 100 μM AZ1, 10 μM NA1 and 100 μM AZ2 (see **Experimental section**, NA1 was measured at 10 μM for a better exhibition of the conductance features) dissolved in a mixed solvent of tetrahydrofuran and mesitylene (1:4). The measurement generated conductance vs. distance traces (**Figs. 2a, 2d and 2g**) during tip retractions, showing plateaus associated with the formation and breakdown of Au-molecule-Au junctions. Plateaus at two discrete conductance levels can be repeatedly observed on individual traces for all three molecules. By overlaying thousands of individual conductance vs. distance traces without selection, we constructed the two-dimensional (2D) conductance vs. distance histograms (**Figs. 2b, 2e and 2h**). In accordance with the two-level plateaus on individual traces, each 2D histogram displays two high count regions: the high conductance (HC) state and the low conductance (LC) state, revealing the existence of two different types of junctions.

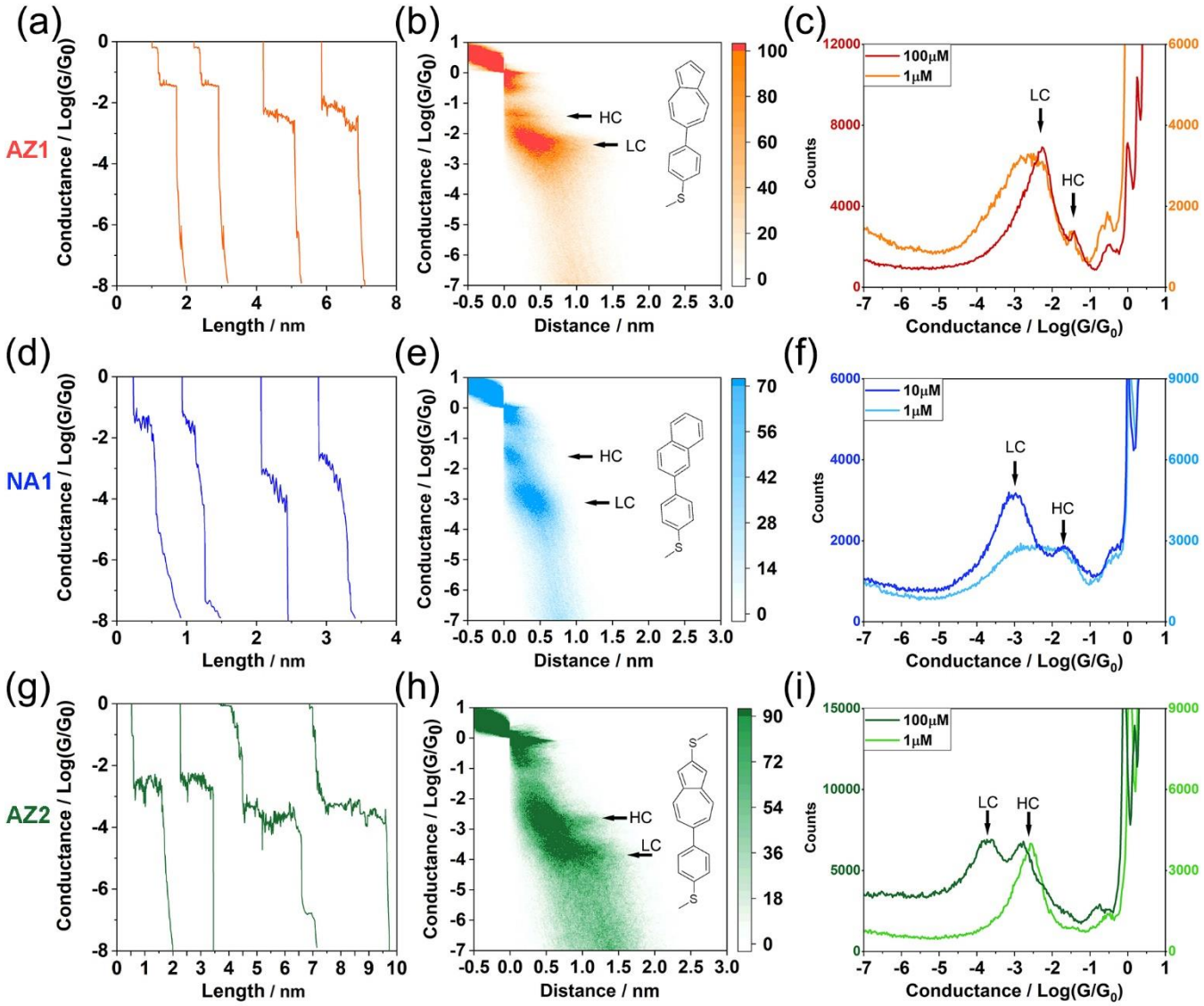

**Figure 2. Conductance measurements of AZ1, NA1 and AZ2.** **(a-c)** Measurements of 100 μM AZ1: **(a)** representative individual conductance vs. distance traces, **(b)** two-dimensional (2D) conductance vs. distance histogram and **(c)** One-dimensional (1D) conductance histogram; **(d-f)** Measurements of 10 μM NA1: **(d)** individual conductance traces, **(e)** 2D conductance histogram and **(f)** 1D conductance histogram; **(g-i)** Measurements of 100 μM AZ2: **(g)** individual conductance traces, **(h)** 2D conductance histogram and **(i)** 1D conductance histogram. Different concentrations are represented by different colors as the insets indicate. The black arrows mark the conductance states at high conductance levels (HC) and low conductance levels (LC). Each histogram is constructed from over 3000 curves without data selection. The tentative interpretations of the junction configurations are shown in **Table 1**.

---

We then proceeded to conductance measurements at lower concentration (1 μM) for AZ1, NA1 and AZ2 (**Figs. S1a-c**), and constructed the one-dimensional (1D) conductance histograms for both high (10 and 100 μM) and low (1 μM) concentrations as shown in **Figs. 2c, 2f and 2i.** For better comparison of the relative change between the HC and LC peaks, the 1D histograms at different concentrations are normalized by the HC peak height. According to previous studies, the effect of π-π stacking is closely dependent on molecular concentration [27-30]. At high concentrations, the 1D histogram of each structure features two peaks (HC and LC) corresponding to the two high count regions in 2D histograms. In addition, for AZ1 and NA1, the LC peaks were higher in count than the HC peaks, while for AZ2, the LC and HC peaks were comparable. Upon decreasing the concentration, the LC peak changed relative to the HC peak in three different patterns: it vanished for AZ2, the area under the peak decreased for NA1 and it broadened for AZ1. The HC peaks, were independent of the concentration and can be attributed to single-molecule (monomer) junctions formed by two Au-S contacts for AZ2 or by Au-S and Au-π contacts [31, 32] for AZ1 and NA1. In contrast, the concentration dependency of the LC peaks of NA1 and AZ2 indicates that the LC peaks were formed fromπ-stacked dimers, whose formation probability significantly depends on the concentration [29, 30]. For AZ1, based on the similarity in molecular structure and two-peak pattern between AZ1 and NA1, we inferred that the LC peak of AZ1 was also due to π-stacked dimers. The lack of obvious concentration dependence of the AZ1 LC peak was possibly due to the exceptionally strong π-π stacking of the azulene-based aromatic structures even at low concentrations. In contrast with AZ1, the HC state of AZ2 was more dominant at both high and low concentrations, in agreement with the reasoning that double Au-S contacts provided more stable and more-probable monomer junctions compared to the π-stacked dimers. Clearly, at high concentrations, the LC state was more evident than the reported stacked dimers of nonpolar π structures [29, 30], suggesting stronger π-π interactions between the azulene-based π structures. The more intense intermolecular activity for AZ1 (or AZ2) than NA1 revealed by single-molecule measurements is supported by the DLS analysis (**Fig. S2** and **Table S1**), and beyond the detection capability of UV-Vis adsorption spectroscopy at comparable concentrations (**Fig. S3**).

The above reasoning is supported by the conductance values (**Table S2**). At high concentrations where both HC and LC peaks can be clearly resolved, the most-probable HC value of AZ1 ($3.73\times10^{-2}$ $G_0$, $G_0$ for the quantum conductance, 77.6 μS) was slightly higher than that of NA1 ($2.11\times10^{-2}$ $G_0$), consistent with the similar junction contacts and configurations predicted for AZ1 and NA1 monomers. But the most-probable low conductance value of AZ1 ($4.33\times10^{-3}$ $G_0$) was ~5 times of that of NA1 ($9.34\times10^{-4}$ $G_0$), revealing evidently higher charge transport efficiency, possibly due to the better coupled π-π system. In comparison, AZ2 displayed lower HC and LC values ($1.65\times10^{-3}$ $G_0$ and $1.93\times10^{-4}$ $G_0$). This could be a consequence of sulfur on the 2-position of azulene affecting the molecular energy level and also inducing sulfur-π interaction with the phenyl ring on the other monomer [33]. The attribution of peaks and evaluation of π-π stacking strength is validated by the following analysis and theoretical calculations.

As control experiments, pure solvent was measured for the calibration of background and single molecules in self-assembled monolayers (SAMs) without solvent were measured to determine the intrinsic conductance features of AZ1 and NA1 (**Fig. S4**). The break junction measurement of pure solvent showed no plateaus in individual conductance traces or peak in conductance histograms. On the other hand, for AZ1 and NA1 in SAMs without solvent, the single-molecule conductance measurement displayed HC and LC conductance features for both molecules, of which the conductance values were similar to those measured in solution. The control experiments corroborated the origin of conductance features of the studied molecules.

To provide further evidence for the attribution of conductance peaks, we conducted statistical analysis for the size of the STM tip-substrate gap for AZ1, NA1 and AZ2. We calculated the distance from the breakdown of Au-Au quantum contact to the breakdown of HC/LC plateaus on each conductance vs. distance traces (see details in **Experimental section** and **Fig. S5a**), and constructed histograms showing the distribution of total tip displacements for the HC (**Fig. S5b**) and the LC (**Fig. 3a**) states. The size of the tip-substrate gap was estimated by adding a 0.5 nm snap-back distance [34, 35] to the averaged tip displacement. For the HC states, the averaged gap size at the breakdown was determined to be 0.878 nm, 0.912 nm

and 1.117 nm for AZ1, NA1 and AZ2, respectively. The gap sizes for AZ1 and NA1 were slightly shorter than their molecular lengths (0.924 nm and 1.081 nm), as expected for monomer junctions with Au-S covalent coupling on one side and a 'point to face' Au-π coupling on the other side. The gap size for AZ2 was about the same as its molecular length (1.104 nm), consistent with single-molecule junctions formed by covalent contact on both ends. In comparison, for the LC states, the averaged gap size was 1.214 nm, 1.131 nm and 1.383 nm for AZ1, NA1 and AZ2, respectively, all of which were longer than the corresponding molecular lengths, confirming that π-stacked dimers were the origin of the LC states. In particular, the gap size of AZ1 and NA1 were consistent with their theoretical junction lengths, estimated for the fully stacked configurations (1.214 nm and 1.224 nm, DFT optimizations shown in later section) with both the phenyl ring and the azulene/naphthalene group stacked. The more extended gap size of AZ2 suggests that the second -SMe group elongated the dimer junction by participating in the π-π interaction, which is in agreement with the decreased low conductance values.

To examine the influence of twist angle on molecular conductance and π-π interaction, we performed DFT calculations of the energy of AZ1 and NA1 as a function of their twist angle (**Fig. S6**). On one hand, as reflected in the energy profile, the twist angles for the optimized conformations of AZ1 and NA1 are **35°** and **30°**, respectively. The slightly larger twist angle of AZ1 is potentially due to the stronger steric repulsion between the larger seven membered ring and the adjacent phenyl ring. Although the difference in twist angles is moderate, according to the reported relation, the slightly larger twist angle in AZ1 does not account for our observations, because it should theoretically weaken π-π stacking [36, 37] and suppress molecular conductance [38, 39]. In contrast, we observed stronger π-π stacking and higher conductance for monomers and dimers of AZ1 than NA1, which is in the opposite trend of the twist angle effect.

On the other hand, the conductance measured at room temperature is a thermally averaged result with twist angles changing dynamically on a fs ($10^{-15}$ s) time scale. A larger probability to achieve the coplanar configuration (0º twist angle) also points to a higher averaged conductance. We characterized this probability by calculating the energy barrier between 0º and the optimal twist angle. As illustrated in **Fig. S6**, $\Delta E_{AZ1}$ is about 0.2 eV and $\Delta E_{NA1}$ is about 0.07 eV, suggesting larger probability for NA1 to achieve the coplanar, higher conductance configuration. Both the above two effects caused by twist angle predict higher conductance and stronger π-π stacking of NA1 than AZ1, which is the opposite of our experimental observation. Therefore, we can exclude twist angle as the reason for the enhancement of conductance and π-π interaction.

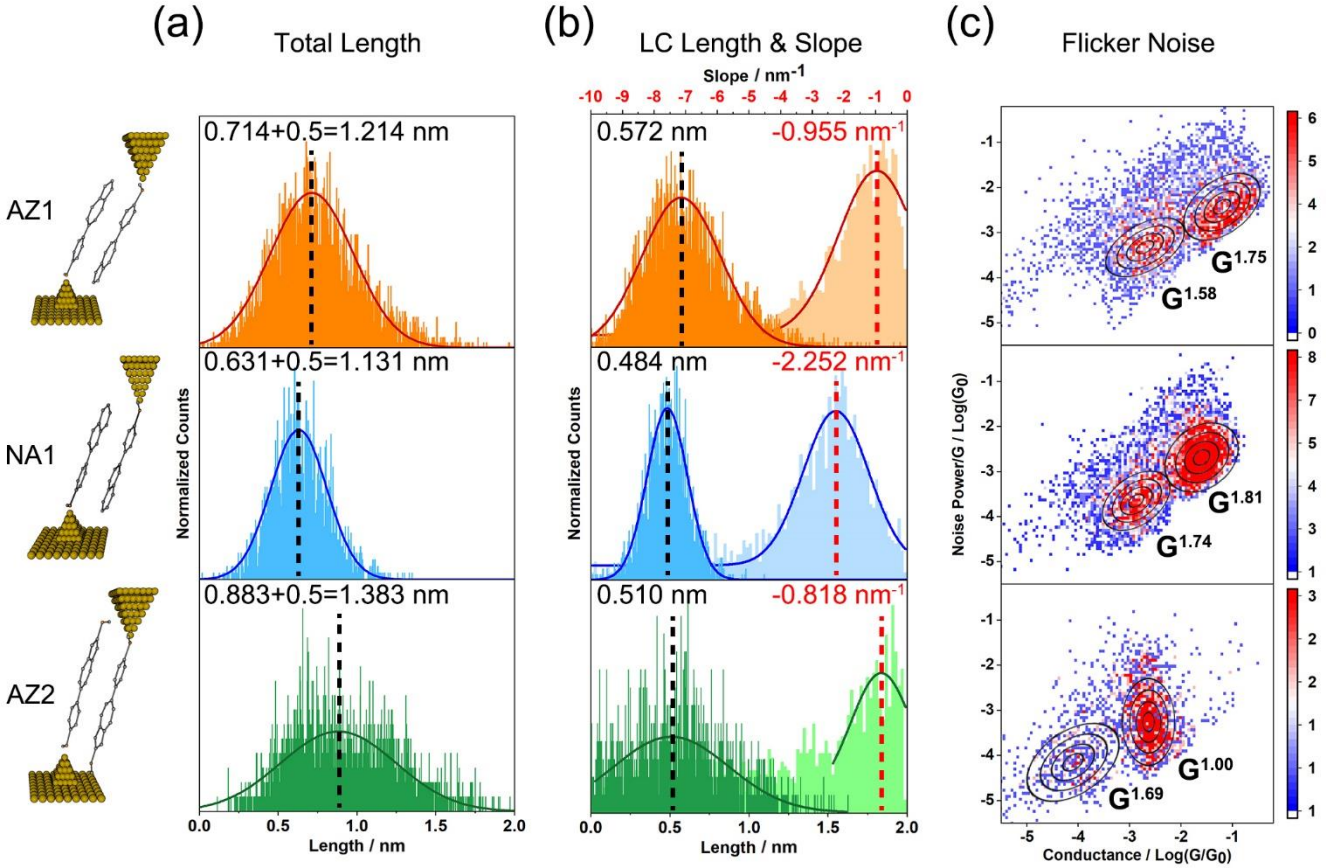


**Figure 3. Analysis of the tip-substrate gap size, conductance plateau length and slope, and flicker noise power.** **(a)** Distribution of total tip displacement for AZ1, NA1 and AZ2. The estimated tip-substrate gap size is marked in each panel. **(b)** Distribution of low conductance (LC) plateau length and slope for AZ1, NA1 and AZ2. The dashed lines and numbers indicate the fitted Gaussian positions of the length (black) and slope (red). See **Experimental section** for detailed methods for the statistical analysis. **(c)** Two-dimensional histograms of normalized flicker noise power against conductance for AZ1, NA1 and AZ2. Each data point corresponds to a 0.2 s tip halted conductance trace. The noise power scales as annotated in the graph.

---

Plateau length/slope and flicker noise analysis also indicate strong π-π stacking between azulene-based molecules

After determining the conductance features of the π-stacked dimers, we then evaluated the strength of π-π stacking in detail by statistical analysis of the plateau lengths and slopes of the LC states of AZ1, NA1 and AZ2. The plateau length represents the tip displacement from the formation to the breakdown of a specific junction configuration, which is determined by the lifting and stretching of the junction during the tip retraction. Because all the studied π-stacked dimers anchor to the electrodes via the same Au-S contacts, the mechanical stability of the π-π interaction between single molecules can be extracted and directly compared. We calculated the plateau length from each conductance vs. distance trace according to the 3σ limits (see **Experimental section**), and constructed histograms showing the distributions of LC plateau lengths (**Fig. 3b**). Remarkably, the averaged LC plateau length of AZ1 (0.572 nm) was larger than that of NA1 (0.484 nm), revealing higher stability and coupling strength of π-π stacking between azulene-based molecules than between naphthalene-based molecules. The LC state of AZ2 exhibited a shorter plateau length (0.510 nm) than AZ1, but longer than NA1. This indicates that the inclusion of the –SMe substituent weakened the stacking of azulene-based molecules, but still maintained a stronger stacking than that of the naphthalene-based, nonpolar π structures.

The plateau slope measures the change in junction conductance during tip retraction, and is an indicator of the electronic coupling in response to mechanical stretching of molecular junctions [40]. We analyzed the plateau slope from the measured conductance vs. distance traces according to the 1σ limit (see **Experimental section**) and constructed histograms showing the distributions of LC plateau slopes (**Fig. 3b**). The averaged

LC plateau slope for NA1 (-2.252 $nm^{-1}$) was significantly larger than those of AZ1 (-0.955 $nm^{-1}$) and AZ2 (-0.818 $nm^{-1}$), confirming the higher mechanical stability of π-π electronic coupling between azulene-based structures than that between naphthalene-based structures. To rationalize the origin of the slope difference, we consider a mechanical model of π-stacked dimer junctions, as described in **Fig. S7**. Assuming the energy barrier originating from the contacts, the monomers, and the π-π stacking, the Landauer-Buttiker formalism [41, 42], combined with phase-coherent tunneling, relates the conductance ($G$) of the π-stacked dimer junction to the decay constants ($\beta_{c/m/\pi}$, where c, m and π represent contact, monomer and π-π stacking, respectively) and barrier widths ($L_{c/m/\pi}$) via the expression $G \propto e^{-\beta_c L_c} \cdot e^{-\beta_m L_m} \cdot e^{-\beta_\pi L_\pi}$ [43]. Thus the LC plateau slope is expressed as [40]

$$\left|\frac{\Delta(Log\ G)}{\Delta L}\right| \propto \beta_c \frac{\Delta L_c}{\Delta L} + \beta_m \frac{\Delta L_m}{\Delta L} + \beta_\pi \frac{\Delta L_\pi}{\Delta L} \quad \textbf{Eq. 1}$$

With the stretching distance components ($\Delta L_{c/m/\pi}$) expressed by the force ($F$) and the corresponding spring constants ($k_{c/m/\pi}$), and assuming similar $k_{c/m}$ and $\beta_{c/m/\pi}$ for AZ1 and NA1, the ratio of the LC plateau slopes of AZ1 and NA1 is described by

$$\frac{\left|\frac{\Delta(Log\ G_{AZ1})}{\Delta L}\right|}{\left|\frac{\Delta(Log\ G_{NA1})}{\Delta L}\right|} \approx \frac{\frac{\beta_c}{k_c}+\frac{\beta_m}{k_m}+\frac{\beta_\pi}{k_{\pi,AZ1}}}{\frac{\beta_c}{k_c}+\frac{\beta_m}{k_m}+\frac{\beta_\pi}{k_{\pi,NA1}}} \quad \textbf{Eq. 2}$$

Since it is apparent that $\frac{\beta_c}{k_c} + \frac{\beta_m}{k_m} > 0$, by substituting the slope values, one obtains $\frac{k_{\pi,AZ1}}{k_{\pi,NA1}} > \frac{0.955\ nm^{-1}}{2.252\ nm^{-1}} = 2.36$, so $k_{\pi,AZ1} \gg k_{\pi,NA1}$. The larger $k_\pi$ of AZ1 suggests a stiffer stacked π system and stronger coupling comparing to that of NA1. The ratio of breakdown force ($F_{break,AZ1/NA1}$) of the LC plateaus can be further estimated by the total spring constants ($k_{AZ1/NA1}$) and the measured stretching distance ($\Delta L_{AZ1/NA1}$) as

$$\frac{F_{break,AZ1}}{F_{break,NA1}} = \frac{k_{AZ1} \cdot \Delta L_{AZ1}}{k_{NA1} \cdot \Delta L_{NA1}} \quad \textbf{Eq. 3}$$

Based on the conclusion from **Eq. 2**, we have $k_{AZ1} > k_{NA1}$ (assuming similar $k_{c/m}$) and the LC plateau length distribution in **Fig. 3b** shows that $\Delta L_{AZ1} > \Delta L_{NA1}$. We therefore conclude that $F_{break,AZ1} > F_{break,NA1}$. The above mechanical model corroborated stronger π-π stacking for AZ1 dimers than NA1 dimers from the both the spring constants and the breakdown forces.

On the other hand, we performed the same analysis of the plateau length and slope of the HC states of AZ1, NA1 and AZ2 (**Figs. S5c and d**). The large plateau length (0.448 nm) and shallow plateau slope (-0.451 $nm^{-1}$) of AZ2 support the monomer's covalent binding to both electrodes [40]. In contrast, NA1 and AZ1 exhibited similar, shorter plateau length (0.365 nm and 0.308 nm), but the slope of AZ1 (-0.410 $nm^{-1}$) was smaller than that of NA1 (-1.280 $nm^{-1}$), reflecting a stronger Au-π coupling possibly due to the excessive negative charge on the five-membered ring.

To gain further insight into the electronic coupling strength of π-π stacking, we conducted flicker noise analysis on AZ1, NA1 and AZ2. Flicker noise (1/f noise) comes from the electronic fluctuations on the electrodes, which are affected by the coupling along the charge transport pathway. The analysis of flicker noise has been proved to be effective in studying the electrical coupling mode of molecular junctions [44-47]. The flicker noise power (PSD) is proportional to the $n$-th power of junction conductance: $n = 1$ when the charge transport is dominated by through-bond coupled pathway, and $n = 2$ when through-space transport dominates. In our experiment, we stopped the tip movement upon detection of a molecular junction, and collected the tunneling current for 0.2 s, from which the flicker noise (100-1000 Hz) was extracted and analyzed. **Fig. 3c** shows the histograms of normalized PSD vs. conductance (detailed analytical method in **Experimental section**). For the HC states, the PSD of AZ1 and NA1 scaled with $G^{1.75}$ and $G^{1.81}$, respectively. The $n$ values were close to the through-space coupled situation and in agreement with those reported for Au-π coupling [44]. In contrast, the PSD of the HC state of AZ2 scaled with $G^{1.00}$, revealing a through-bond coupling mechanism that was reported for Au-S anchored molecules [44, 48, 49]. The above characteristics confirmed the proposed configurations of the monomer junctions. For the LC states, the PSD of NA1 scaled with $G^{1.74}$, typical of previously studied nonpolar π-π interactions [29]. Interestingly, the LC states of AZ1 and AZ2 exhibited lower $n$ values (1.58 and 1.69) that are more prone to through-bond coupling in comparison with NA1. The flicker noise analysis demonstrates that from NA1 to AZ2 to AZ1, π-π stacking showed increasing strength and emerging features of through-bond fractions. These observations validate the conclusions from the conductance, plateau length and slope analyses.

## Antiparallel alignment of the dipoles contributes to the enhancement of π-π stacking

Having established that azulene showed stronger π-π stacking comparing to naphthalene, we sought to determine the major factor that contributes to the enhancement. Since azulene and naphthalene share identical chemical formulae and similar dimensions, the major distinct difference is their dipole moments (1.08 D for azulene and 0 D for naphthalene), implying that the observed enhancement of π-π stacking stems from the dipole effect. As is well known, dipoles stabilize themselves by changing orientations relative to their neighbors and thus achieving favorable electrostatic interactions. For example, in a simplified two-dipole π-π system, where a face-to-face configuration is favored due to attractive stacking, antiparallel alignment of dipoles is expected to be the configuration with minimum potential energy, as described by the Keesom model [50]. In agreement with this model, antiparallel stacking was also estimated for bulk azulene-based compounds [7, 17]. We therefore reasoned that in our single-molecule measurements, the azulene dipoles adopt similar antiparallel alignment in the π-stacked dimer junctions, and thus the enhancement in π-π stacking

should be sensitive to the relative orientation between the dipoles. To assess this possibility, we designed an asymmetric π-stacked dimer to explore how the stacking strength is dependent on relative rotation between the monomers. We performed the single-molecule conductance measurement of a mixture of the meta-substituted compound, AZ3 (**Fig. 1b**) and AZ1 (100 μM:100 μM). Assuming random stacking among all the molecules, the probability of detecting AZ1 dimers, AZ3 dimers and AZ3+AZ1 dimers should be 25%, 25% and 50%, respectively. For the most detectable type of dimer junctions, AZ3+AZ1, a net torsion force that causes relative rotation of the stacked dipoles should occur as a result of the asymmetric contacting angles of AZ3-electrode and AZ1-electrode. In **Fig. 4a** and **Fig. S8a**, the conductance histogram shows a broadened HC state and a high count LC state. At the breakdown of the LC state, the averaged tip-substrate gap size was 1.160 nm (**Fig. 4b**), which is larger than the size of AZ1 or AZ3 monomers (0.985 nm), indicating dimer configurations. The averaged LC value of AZ3+AZ1 ($2.98\times10^{-2}$ $G_0$, **Table S2**) was moderately lower than that of pure AZ1, potentially resulting from the relatively weaker π-π stacking due to the extra steric repulsion caused by the approximation of the -SMe group on AZ3 to the azulene group of AZ1. The averaged LC plateau length (0.456 nm) was remarkably smaller than that of AZ1 or AZ2, and close to that of NA1. The averaged LC plateau slope (-1.428 $nm^{-1}$) was also deeper than that of AZ1 or AZ2, but shallower than NA1 (**Fig. 4c**). As a control, the pure AZ3 compound was also measured and analyzed by the same procedures (**Figs. S8b-f**). In contrast with the mixture, pure AZ3 showed similarly strong mechanical stability comparing to pure AZ1 during stretching. The above observations identified higher stability upon stretching of π-stacked dimers with symmetric contacting angles (pure AZ3/AZ1) and lower stability of those with asymmetric contacting angles, which involve relative rotation during stretching (AZ3+AZ1 dimer). This phenomenon confirmed dipole interactions as a key contributor to the enhancement of π-π interactions, and supports an optimal antiparallel alignment of the azulene dipoles.

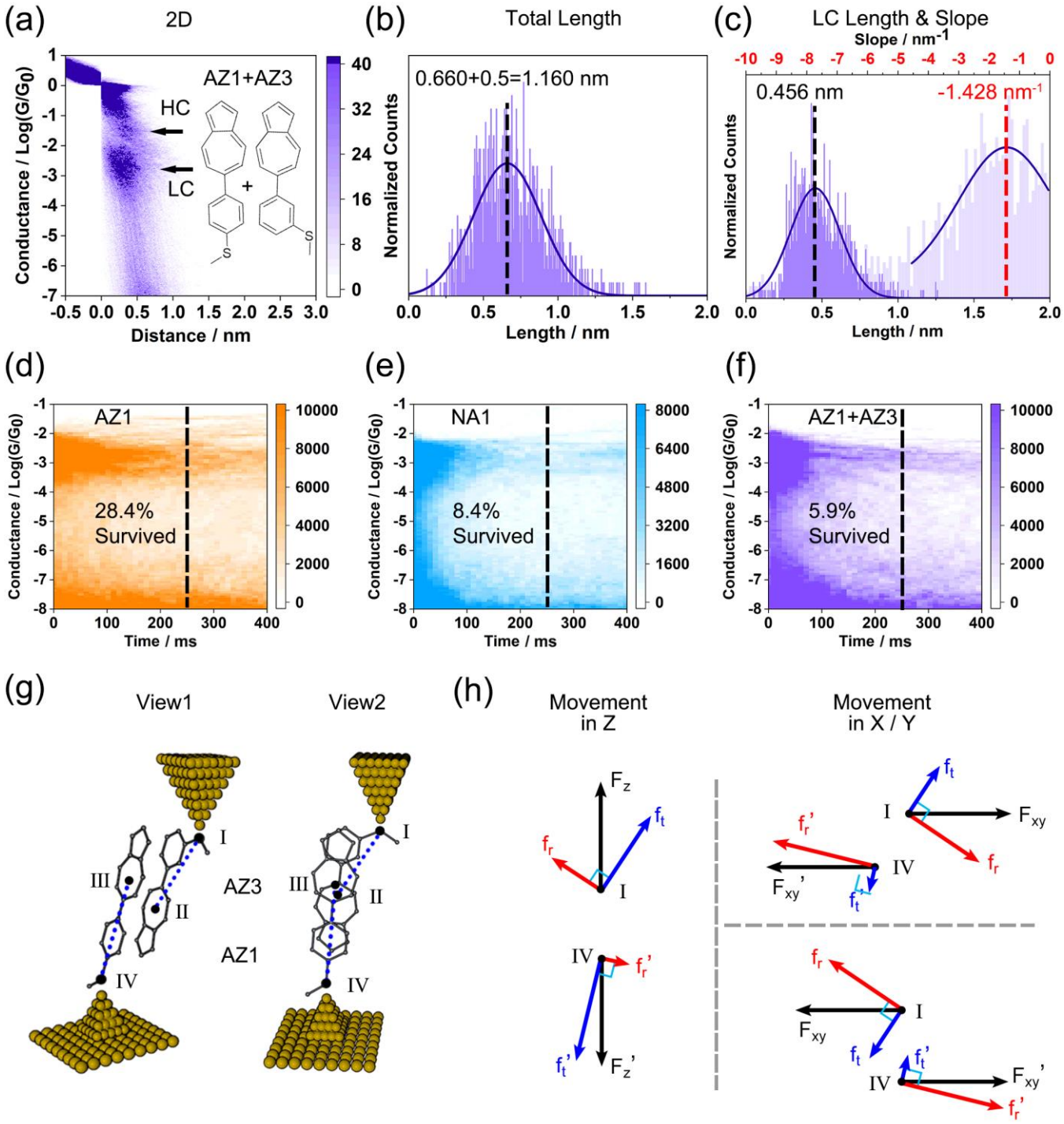


**Figure 4. Dipole assisted π-π stacking in response to rotational force.** **(a)** Two-dimensional conductance vs. distance histograms for the mixed solution of 100 μM AZ1 and 100 μM AZ3 (AZ1+AZ3). **(b)** Distribution of total tip displacement for AZ1+AZ3. The estimated tip-substrate gap size is marked in the panel. **(c)** Distribution of low conductance (LC) plateau length and slope for AZ1+AZ3. The dashed lines and numbers indicate the fitted Gaussian positions of the length (black) and slope (red). **(d-f)** 'Pull and hold' experiments for the LC states of AZ1, NA1 and AZ1+AZ3. Two-dimensional conductance vs. tip halted time histograms for **(d)** AZ1 (100 μM), **(e)** NA1 (100 μM) and **(f)** AZ1+AZ3 (100+100 μM). The dashed lines and numbers show the percentage of survived junctions at 250 ms. **(g)** Schemes of metal-AZ3-AZ1-metal junction observed from two different views. The black dots mark the force-applying position on AZ3 (I), center of the stacked structure of AZ3 (II) and AZ1 (III), and the force-applying position on AZ1 (IV). The blue dotted lines connect the

force-applying position to monomers' joint position. **(h)** Force analysis at positions I and IV for relative electrodes' movement in vertical (Z) and horizontal (X/Y) directions. The overall force (black arrows, $F_{z/xy}$ for I and $F_{z/xy}$' for IV) applied on the molecule-electrode contact is decomposed into the force for translational motion (blue arrows) and rotational motion (red arrows). Force analysis shows that the rotational forces on AZ1 and AZ3 are not anti-symmetric, from which relative rotation will occur between the stacked azulene units.

---

We further carried out a 'pull and hold' experiment on AZ1, NA1 as well as the AZ1+AZ3 mixture to test the mechanical stability of the π-stacked dimers in response to a random force by the tip drift. We held the tip for 0.4 s upon detecting the LC states, and constructed 2D conductance vs. time histograms (**Figs. 4d-f**) from thousands of *G-t* traces. The histograms reveal two distinct bands at the LC level and at the background noise level, representing the breakdown of molecular junctions during the tip holding. By comparing the conductance histograms at $t$ = 0 and $t$ = 250 ms (**Figs. S9a-c**), we resolved the survival of 28.4% of AZ1 dimers, 8.4% of NA1 dimers and 5.9% of AZ3+AZ1 mixed dimers. The evidently higher survival rate of AZ1 dimers than NA1 dimers proves the dipole-induced enhancement of π-π stacking. Intriguingly, the survival rate of AZ3+AZ1 mixed dimers was even slightly lower than NA1 dimers, indicating weak mechanical stability of asymmetric contacting dimers upon random stretching/compressing forces due to tip drifting (explained by force analysis in the following paragraph). Note that the survival rate of AZ3+AZ1 mixed dimers was less than half of the rate of AZ1 dimers. Considering the fact that AZ3 dimers displayed comparable mechanical dependency of stacking strength with AZ1 dimers (**Figs. S8b-f**), we infer that more than 50% of the detected dimers are formed between AZ3 and AZ1, which could be reasonably attributed to the potentially different binding affinities of AZ3 and AZ1 to the substrate.

To interpret the anisotropy of the mechanical stability of dipole-assisted π-π stacking, we performed force analysis for the AZ1+AZ3 dimer bridged between the two STM electrodes. **Fig. 4g** illustrates two different views of a representative configuration of the stacked dimers. By assuming negligible deformation within each monomer, the situation can be simplified to the relative motion of AZ3 and AZ1 in response to a pair of force applied on positions I and IV. The stacking centers of AZ3 (II) and AZ1 (III) are dynamically joined by π-π interaction. As shown in **Fig. 4g**, the connecting line from I to II is not in parallel with that from IV to III, because of the asymmetric electrode-contacting angles of AZ3 and AZ1. We then analyzed the forces on positions I and IV due to possible tip-substrate relative movement in vertical (Z) and horizontal (X/Y) directions (**Fig. 4h**). The overall force ($F_{z/xy}$, $F_{z/xy}$') is decomposed into the force for translational motion ($f_t$, $f_t$') and the force for rotational motion ($f_r$, $f_r$'). $f_t$ and $f_t$' only lead to translational movement between the monomers, but $f_r$ and $f_r$' give rise to the rotation of the stacked π systems. In particular, when $f_r$ and $f_r$' are antiparallel and of the same amplitude, the dimer is expected to rotate as a unit and only translational separation occurs; when $f_r$ and $f_r$' are not anti-symmetric, as in the case here for AZ3 and AZ1, the relative rotation will take place between the stacked parts. As a result, the antiparallel alignment of the dipoles is disturbed, explaining the weakening of the mechanical stability of π-π stacking between AZ3 and AZ1. Moreover, the distinct mechanical properties under translational vs. rotational intervention offer multi-dimensionally switchable device functions.

Previous theoretical studies and experimental studies have suggested antiparallel stacking of polar aromatic groups [7, 17], which supports the dipole-assisted π-π stacking observed in this study. Nevertheless, the formation of a crystal is a cooperative consequence of complicated interactions among a large quantity of molecules, thus making it difficult to disentangle dipole interactions from other influences. In the current work, we directly studied the dipole effect on π-π interactions by probing the stacking between two single molecules anchored to the two STM electrodes. Furthermore, we rotated the dipoles and studied the orientation-dependency of the stacking strength. Interpretation and controlling of the dipole effect were achieved here by single-molecule conductance measurements. Nevertheless, complete deconvolution of dipole interactions from π-π stacking remains a colossal task to be pursued in the future, which requires profound exploration on the influence from solvent, temperature, electrode, etc.

## Theoretical calculations

To shed further light on the experimental observations, we evaluated the optimal stacked geometries and calculated their transmission functions, $T(E)$, by combining the density functional theory (DFT) [51, 52] with the quantum transport code, Gollum [53]. The electronic structures of AZ1 and NA1 monomers were first investigated (**Fig. S10**). The frontier orbitals closest to the Fermi energy, which provide the most significant contributions to transport are the delocalized HOMO and LUMO of NA1 and the delocalized HOMO-1 and LUMO of AZ1. Although the localized HOMO of the latter does not contribute to electron transport, the calculated HOMO-1-LUMO gap of AZ1 (2.14 eV) is smaller than the HOMO-LUMO of NA1 (2.64 eV), which explains the moderately higher conductance for AZ1. This is further demonstrated by the calculated transmission functions for NA1 and AZ1 monomers (**Fig. S11**). In the case of stacked dimers, the

DFT optimization of the configurations suggests that the two monomers are fully stacked in an antiparallel arrangement, as shown in top left of **Fig. 5a**. Moreover, the calculated junction length of the optimized fully stacked dimer configurations (1.214 nm for AZ1 and 1.224 nm for NA1) are in agreement with the experimentally measured tip-substrate gaps for the LC states (1.214 nm for AZ1 and 1.131 nm for NA1).

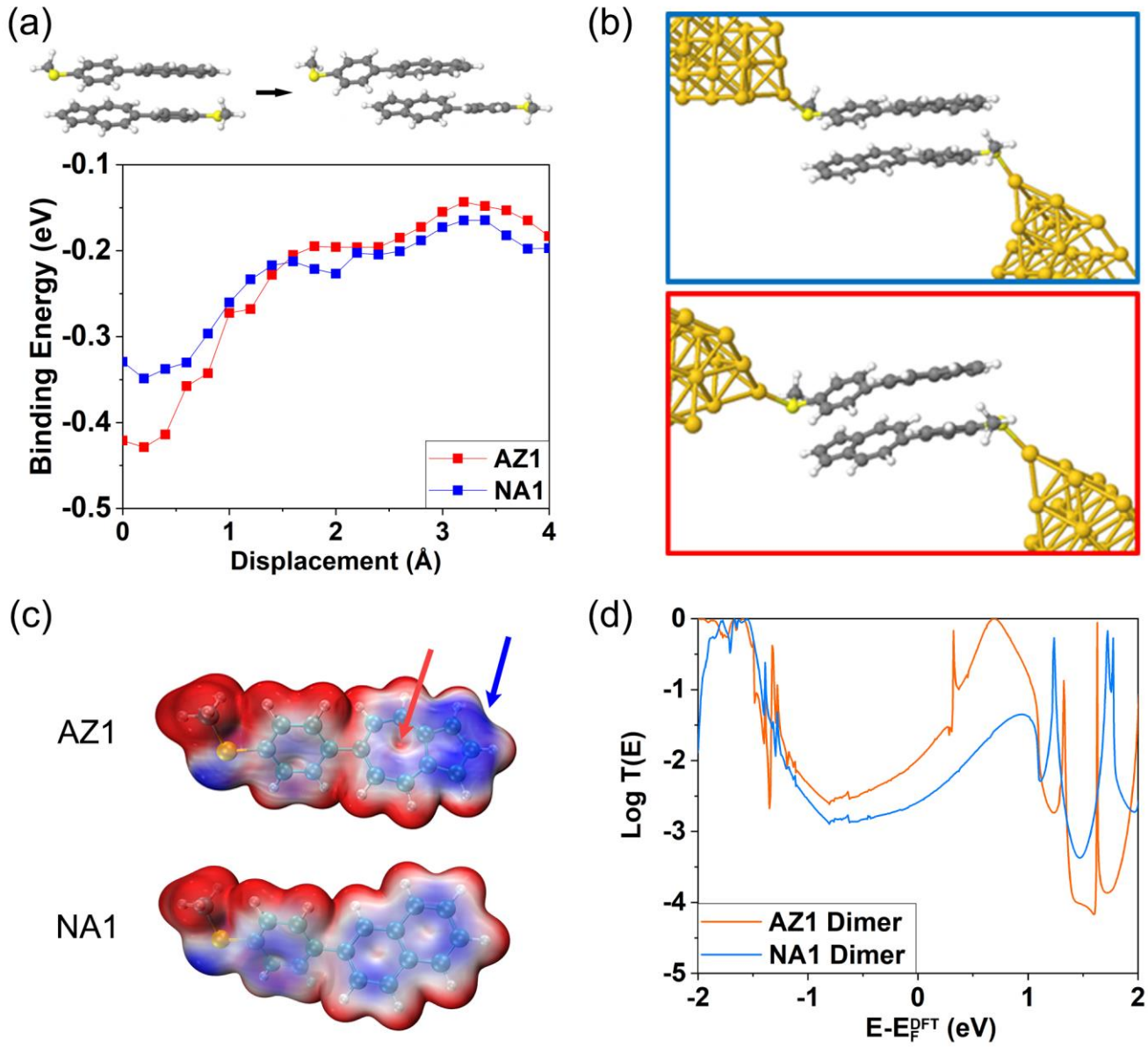


**Figure 5. Transport properties of stacked AZ1 and NA1. (a)** Binding energy as a function of stretching distance of fully stacked AZ1 dimers and NA1 dimers. **(b)** Calculated optimal conformations for fully stacked AZ1 (top) and NA1 (bottom) attached to two electrodes. **(c)** Electrostatic potential of monomer AZ1 and NA1. Positive and negative potentials are indicated by red and blue, respectively. **(d)** Calculated transmission functions for the stacked AZ1 and NA1 dimers.

The proposed stacking configuration is supported by our calculated binding energy (BE) as a function of displacement in the antiparallel direction (**Fig. 5a**, bottom). The stretching was performed by shifting the top monomer from 0 to 4 Å, with an interval step of 0.2 Å, and fully relaxing the geometries at each step. For both AZ1 and NA1, the BE decreases with the shrinking overlap area of the two monomers. A higher BE indicates that there will be a higher probability for the dimer conformation to be measured in experiments. Therefore, the antiparallel, fully stacked dimers are employed to model the experiment (**Fig. 5b**). In particular, the fully stacked AZ1 dimer shows

a higher BE (-0.43 eV) than the NA1 dimer (-0.35 eV), signaling a stronger π-π interaction between the AZ1 monomers, in agreement with our experiments. It is interesting to clarify the contribution from electrostatic interaction of two azulene monomers during this pulling process. We therefore stretch the two monomers apart further until 12 Å (**Fig. S12**). At a displacement distance around 6 Å, the two antiparallel stacked azulene units are fully overlapped. The whole process is divided to three regions as indicated by the shaded areas in **Fig. S12**. The electrostatic contributions are rationalized by noting that the seven-membered ring is positive charged while the five-member ring is negative charged for azulene. In region A where the two azulenes are approaching each other, the two seven -member rings are moving closer introducing a repulsion between the two monomers resulting in a weaker binding compared with NA1 dimer. However, in region B, where the two azulenes are close to being antiparallel stacked, the five-membered ring at the bottom (top) and the seven-membered ring on the top (bottom) attract each other, leading to stronger binding energy than NA1. In region C, at the final stage of stretching, the two five-member rings repel each other slightly, which weakens the interaction between the two monomers.

The stronger interaction between AZ1 monomers can be further rationalized by analyzing the electrostatic potential (ESP) of AZ1 and NA1 (**Fig. 5c**). For AZ1, a strong negative potential is observed on the five membered ring (blue arrow) and a slight positive potential is present in the center of the seven-membered ring (red arrow), consistent with an intramolecular dipole in AZ1. In contrast, no obvious potential difference is obtained across the aromatic structure of NA1. The potential distribution on AZ1 supports the view that electrostatic interactions between two molecules can enhance the π-π stacking in favorable orientations. The enhancement was also correlated with the energy level splitting of dimer compared with its counterpart monomer, since the electronic coupling between the frontier orbitals of two monomers could be estimated by the splitting of their energy level into bonding and anti-bonding combinations. **Fig. S13** and **Fig. S14** show that the splitting of the LUMO and LUMO+1 of the NA1 dimer are 0.05 eV and 0.02 eV respectively, which are significantly smaller than those of AZ1 dimer (0.44 eV and 0.31 eV). The difference in energy splitting indicates a stronger interaction between the two AZ1 monomers, resulting in a greater reduction of the HOMO-LUMO gap of the AZ1 dimer. Finally, based on the transmission functions of AZ1 and NA1 dimers (**Fig. 5d**), it is evident that the AZ1 dimer has a higher conductance than the NA1 dimer over the whole energy range of HOMO-LUMO gap, due to its smaller HOMO-LUMO gap. Therefore, our calculations support the antiparallel, fully stacked configurations for AZ1 and NA1, and explain the experimentally observed stronger π-π interaction and higher conductance for the stacked AZ1 dimers compared with the NA1 dimers. Based on Koopmans' theorem, the transfer integral is equal to half of the energy splitting of dimer between LUMO and LUMO+1 or HOMO-1 and HOMO. More straightforward calculation for transfer integral between monomer molecular orbitals is also proposed by the literature [54]. Therefore in order to further stress the contribution of transfer integrals, we directly calculated it via $\langle \phi^1_{LUMO} | F | \phi^2_{LUMO} \rangle$ where $\phi^1_{LUMO}$ and $\phi^2_{LUMO}$ are the LUMOs of two monomers (AZ1 or NA1 in current work) [55], since DFT-predicted Fermi energy is located close to LUMO indicating electron transport. In this expression, $F = SC\varepsilon C^{-1}$ is the Fock operator of the dimer, where $S$ is the inter-molecular overlap matrix, $C$ and ε are the molecular orbitals' coefficients and eigenvalues respectively. We find that half of the energy splitting (0.22eV for AZ1 dimer and 0.025eV for NA1 dimers) is very close to the directly calculated transfer integral (0.221eV for AZ1 dimer and -0.01eV for NA1). To conclude, the transfer integral of the AZ1 dimer is much greater than that of the NA1 dimer indicating better charge transfer performance of the AZ1 dimer, which again support our conductance measurement, where the AZ1 dimer possesses a higher conductance.

It is interesting to observe that the conductance of AZ2 (two Au-S contacts) is lower than that of AZ1 (Au-S and Au-π contacts). To understand this feature, we first carried out a transport calculation for AZ2, and compared it with that of AZ1 (four types of Au-π contacts are considered). All the molecules in junctions are fully relaxed. As demonstrated in **Fig. S15**, AZ2 shows a lower conductance compared to that of AZ1 in the energy region close to Fermi level (gray shaded region). The high conductance of AZ1 can be attributed to its closer located LUMO resonance and the relatively strong Au-π coupling. As shown in **Fig. S15**, the calculated binding energies of Au-π contacts (-0.86 eV ~ -1.45 eV) are on average larger than that of Au-S contacts (-0.86 eV). The strong Au-π coupling thus contributes to the higher conductance of AZ1. The high charge injection efficiency through Au-azulene coupling is also confirmed as shown in **Fig. S16** by the comparison between a molecule with azulene at both ends (DAZ) and its counterpart with -SMe at both ends (DAZS). The conductance enhancement due to direct charge injection into the π system was also reported by Mads et al [56].

The junctions in cofacial contacting conformations (AZ1-c01 and AZ1-c02) showed even higher conductance and larger binding energy (-1.29 eV and -1.45 eV) compared to those in non-cofacial conformations (-0.86 eV and -1.22 eV), suggesting a considerable probability for AZ1 to be measured in a cofacial geometry that features even higher conductance. The same trend potentially applies to NA1 as well. Note that in a real experiment the measured conductance should be obtained from an ensemble of all possible contacting conformations.

To shed light on the conductance difference between the AZ1 dimer and the AZ2 dimer, we first calculated the transmission functions of the optimized AZ1 and AZ2 dimers (**Fig. S17**). AZ1 dimer shows a higher conductance than the AZ2 dimer due to the smaller HOMO-LUMO gap (1.53 eV vs.1.72 eV). Furthermore, we studied the π-π interaction from a dynamic viewpoint, where we fixed the bottom monomer and rotated the -SMe groups in the top molecule. The binding energy as a function of the vertical distance between the two monomers are examined (**Figs.**

**S18a** and **S18b**). The extracted optimal distances are larger for the AZ2 dimer than for the AZ1 dimer as shown in **Fig. S18c**, indicating weaker π-π stacking for AZ2 than AZ1. This is further verified by the more rapidly decreasing binding energy of the AZ2 dimer than the AZ1 dimer while progressively varying the rotation angle with the fixed optimal vertical distance (**Fig. S18d**). The weakening of stacking due to the steric hindrance caused by side-group rotation is also supported by previous reports [24, 57]. Note that the AZ1 dimer exhibited higher conductance than the AZ2 monomer, which supports the strong π-π stacking for the AZ1 dimer and could also be related with the larger contacting angle of the AZ2 monomer (**Fig. S15**) which therefore weaken the coupling between gold electrode and the π system of monomer AZ2, leading to a lower conductance. To provide intuitive comparison of all the tested species, we summarized the key experimental and calculated data in **Table 1** and extended a discussion for comprehensive interpretation of the data in **Fig. S19**.

**Table 1. The experimental and calculated results of all the tested species**

| | Species | Conductance | PSD | Total Length /nm | Plateau Slope /nm$^{-1}$ | Optimized Conformation | HL Gap /eV | Binding Energy /eV | Calculated G |
|---|---|---|---|---|---|---|---|---|---|
| HC | AZ1 | $3.73\times10^{-2}\ G_0$ | $G^{1.75}$ | 0.878 | -0.410 | 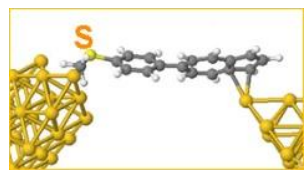 | 1.91 | -0.86 (Au-π) | $1.54\times10^{-1}\ G_0$ |
| | NA1 | $2.11\times10^{-2}\ G_0$ | $G^{1.81}$ | 0.912 | -1.280 | 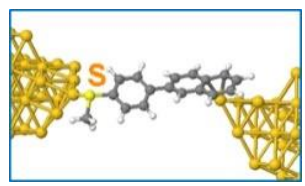 | 2.64 | -0.63 (Au-π) | $1.00\times10^{-2}\ G_0$ |
| | AZ2 | $1.65\times10^{-3}\ G_0$ | $G^{1.00}$ | 1.117 | -0.451 | 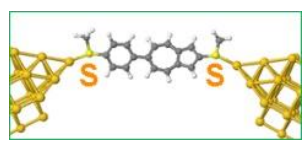 | 1.97 | -0.86 (Au-S) | $2.60\times10^{-3}\ G_0$ |
| | AZ3 | $2.96\times10^{-2}\ G_0$ | / | / | / | / | / | / | / |
| | AZ1+AZ3 | $2.98\times10^{-2}\ G_0$ | / | / | / | / | / | / | / |
| LC | AZ1 | $4.33\times10^{-3}\ G_0$ | $G^{1.58}$ | 1.214 | -0.955 | 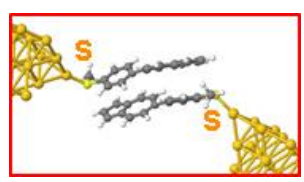 | 1.53 | -0.43 (π-π) | $1.02\times10^{-2}\ G_0$ |
| | NA1 | $9.34\times10^{-4}\ G_0$ | $G^{1.74}$ | 1.131 | -2.252 | 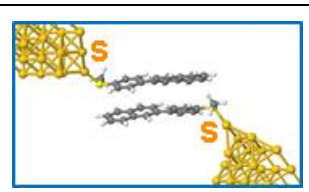 | 2.43 | -0.35 (π-π) | $2.56\times10^{-3}\ G_0$ |
| | AZ2 | $1.93\times10^{-4}\ G_0$ | $G^{1.69}$ | 1.383 | -0.818 | 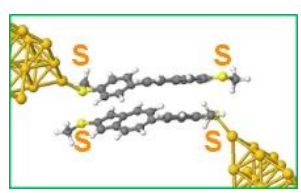 | 1.72 | -0.62 (π-π) | $4.98\times10^{-3}\ G_0$ |

| | | | | | | | | | |
|---|---|---|---|---|---|---|---|---|---|
| | AZ3 | $1.82\times10^{-3}\ G_0$ | / | 1.174 | -1.042 | / | / | / | / |
| | AZ1+AZ3 | $2.35\times10^{-3}\ G_0$ | / | 1.160 | -1.428 | / | / | / | / |

Given that a bias voltage of 0.1 V is applied through a junction gap of around 1 nm in our STM-BJ measurement, the electric field as high as $10^8\ V/m$ could be generated and in principle could affect the molecular conductance. So we evaluated the real dipole and twist angle under this electric field in the transport direction for AZ1 and NA1 (**Table S3** and **Fig. S20**). In an electric field of $10^8\ V/m$, the dipole only changed a small amount for both AZ1 (0.25 D) and NA1 (0.22 D) in comparison to the intrinsic dipole of AZ1. The twist angles of AZ1 and NA1 both decrease with electric field, in agreement with a recent report [36], but the decrease is tiny (0.2º for AZ1 and 0.1º for NA1). Therefore, since these variations are moderate and are in the same trend for AZ1 and NA1, the effect of an electric field is negligible.

## Conclusions

Our work reveals the enhancement of π-π stacking between dipole-bearing molecules. Our single-molecule conductance measurements showed the dipole enhancement of π-π stacking leads to higher conductances, larger plateau lengths, shallower plateau slopes, lower PSD $n$ values and longer junction lifetimes. Mechanical control of the strength of π-π stacking via the relative rotation of dipoles confirmed that the enhancement stemmed from the antiparallel alignment of dipole moments. DFT calculations explained in detail the mechanism of conductance enhancement by dipole-assisted π-π stacking. On the other hand, the measurement of the monomer species revealed high charge transport efficiency via Au-π coupling between the electrode and azulene group, which is also explained by the DFT calculated large binding energy. This work provides single-molecule level strategies for the observation and interpretation of dipole effects on π-π interactions, and point to new applications of dipole-mediated π-π interactions in supramolecular devices and functional materials. In subsequent studies, it would be of interest to design and compare among a library of molecules with similar structures, but different dipoles to explore the quantitative correlation between dipole moment and the strength of π-π stacking.

## Experimental section

### Synthetic procedures and characterizations

The synthetic routes and structures of the AZ-n (n = 1-3) and NA1 molecules are depicted in Scheme S1 in the supporting information. 3- or 4-(methylthio)phenyl substituents were connected to an azulene by Suzuki cross-coupling reaction, and a methylthio group on 2-position of azulene in AZ2 was fixed via $S_NAr$ reaction. UV-vis absorption spectra and cyclic voltammetry (CV) were shown in **Fig. S47** and **Fig. S48**, respectively. The optical gaps ($E_g^{opt}$) were calculated from the onset absorption of the UV-vis absorption spectra, and the optical gaps were 1.67 eV, 1.80 eV, 1.67 eV and 3.46 eV for AZ1, AZ2, AZ3 and NA1, respectively. The HOMO/LUMO energy levels ($E_{HOMO}/E_{LUMO}$) were calculated from the onset oxidation/reduction potentials ($\varphi_{ox}/\varphi_{red}$) in the cyclic voltammograms according to the equations of $E_{HOMO}/E_{LUMO}$ = -e($\varphi_{ox}/\varphi_{red}$ + 4.8 - $\varphi_{Fc/Fc+}$) [58], and the calculated $E_{LUMO}/E_{HOMO}$ were -5.25/-3.69 eV, -5.28/-3.60 eV, and -5.32/-3.72 eV for AZn (n = 1-3). Since no obvious oxidation peak was observed in the cyclic voltammograms of NA1, $E_{HOMO}$ of NA1 cannot be calculated, and the calculated $E_{LUMO}$ of NA1 was -2.86 eV. The optical and electrochemical data were summarized in **Table S4**.

### Conductance measurement

The single-molecule break junction measurements were carried out using a scanning tunneling microscope (STM, Agilent 5500). The STM tip is freshly cut and flamed from a gold wire (0.25 mm diameter, 99.95%, Alfa Aesar). The molecular solution in tetrahydrofuran (THF, 99.9%, Sigma-Aldrich) and mesitylene (TMB, 98%, Energy Chemical) mixed solvent (1:4) was pipetted into the liquid cell on a gold substrate (gold with a thickness of ~160 nm on mica) prepared from vapor deposition under ultrahigh vacuum. During the break junction measurements, the STM tip continuously approached and retracted from the substrate with a procedure described elsewhere [59, 60]. The bias voltage between tip and substrate was set to 0.1V, and the current was collected at a sampling rate of 10 kHz.

### Flicker noise analysis

The conductance data used for flicker noise analysis was collected from an approach similar to STM-BJ. When a molecular plateau is detected during the break junction process, the tip stops moving and remains stationary for 0.2 s, during which the current was recorded at a sampling rate of 100 kHz. A digital band-pass filter of 100 to 1000 Hz was applied to preprocess the experimental data to isolate the effects of low-frequency vibration and high-frequency noise. We removed the parts in the curve which obviously does not belong to the molecular junction to eliminate their interference, most of which are due to breakdown of the junction before reaching 0.2 s. After that, we performed a discrete Fourier transformation on the data and integrated the amplitude in the range of 100-1000 Hz to obtain the noise power of the trace. For each trace, we normalized the noise power by the averaged conductance of that trace, and constructed the two-dimensional histograms of normalized flicker noise power against conductance (**Fig. 3c**).

### 'Pull and hold' experiments

The 'pull and hold' experiments were performed based on the STM-BJ method. During the break junction process, once an LC plateau of π-π stacking was detected, we stopped the tip movement for 0.4 s. The conductance of the molecular plateau was recorded simultaneously at the sampling rate of 100 kHz to produce an individual conductance vs. tip halted time trace. We stacked all the traces and obtained the two-dimensional conductance vs. time (*G-t*) histograms (**Figs. 4d-f**). To resolve the survival rate with time, we plotted the conductance profiles at the $t$ = 0 and $t$ = 250 ms from the 2D *G-t* histograms (**Fig. S9**). The ratio of the Gaussian fitted conductance peak areas at $t$ = 0 and $t$ = 250 ms (A'/A) is determined as the survival rate at 250 ms.

## Statistical analysis of total tip displacement, plateau length and slope

We analyzed the tip displacement, plateau length and slope according to our newly established statistical criteria. We first performed Gaussian fitting for the conductance peaks in the 1D histograms to obtain the peak positions and standard deviations σ, (σ ≈ FWHM/2.355). To precisely calculate the stretching distance and plateau slope, we excluded the curves without junction formation, and calculated the tip displacement from the breakdown of Au-Au quantum contact ($G_0$) to the breakdown of the HC or LC plateau (*G*-3σ) for each curve. For a fair comparison, the criterion was unified according to the corresponding G and σ for each conductance state of all the studied molecules. From thousands of curves, we constructed 1D histograms of total tip displacement at the breakdown of HC (**Fig. S5b**) and LC states (**Fig. 3a**). The gap size between the tip and substrate was estimated by adding the snap-back distance (0.5 nm) to the averaged total tip displacement. The statistical analysis of plateau length was the same as that of total tip displacement except that the calculating range of stretching distance was from *G*+3σ to *G*-3σ, which only included the plateau region. For the statistical analysis of plateau slope, we chose a unified, narrower range from *G*+σ to *G*-σ to avoid error from the pre-plateau and post-plateau sharp decay on the curves.

## DFT calculations

Geometrical optimizations were performed using the DFT code SIESTA [51], with a local density approximation LDA functional, a double-ζ polarized basis, a cutoff energy of 200 Ry and a 0.02 eV/Å force tolerance. In order to compute their conductance, the molecules were each placed between pyramidal Au electrodes. The optimal distance between the Au tip and the S atom was fixed to be 2.4 Å. For each structure, the transmission coefficient $T(E)$ describing the propagation of electrons of energy $E$ from the left to the right electrodes was calculated using Gollum code [53], which combines the mean-field Hamiltonian and overlap matrices of the DFT code SIESTA with Landauer-based quantum transport theory. This is equivalent to using the expression

$$T(E) = \mathrm{Tr}\left[\Gamma_L(E)G_r(E)\Gamma_\mathrm{R}(E)G_r^\dagger(E)\right]$$

where $\Gamma_{\mathrm{L,R}}(E) = i(\Sigma_{\mathrm{L,R}}(E) - \Sigma_{\mathrm{L,R}}{}^\dagger(E))/2$ , $G_r(E) = (g^{-1} - \Sigma_\mathrm{L} - \Sigma_\mathrm{R})^{-1}$, $g$ is the Green's function of the isolated molecule. $\Gamma_{\mathrm{L,R}}$ determines the widths of transmission resonances, $\Sigma_{\mathrm{L,R}}(E)$ are the self-energies describing the contact between the molecule and left (L) or right (R) electrodes. While $G_r$ is the retarded Green's function of the molecule in the presence of the electrodes.

To calculate the binding energy using SIESTA, we employed a counterpoise method to correct for basis set superposition errors that are inherent with the localized orbital basis sets that were employed. In the case of dimers, two monomers were defined as entity A and entity B respectively. The ground state energy for the total system was calculated using SIESTA and was denoted $E_{AB}^{AB}$, with the DFT parameters defined previously. The energy of each entity was then calculated on a fixed basis, which was achieved through the use of ghost atoms. Hence, the energy of one monomer in the presence of the fixed basis was defined as $E_A^{AB}$ and for the other monomer as $E_B^{AB}$. The binding energy (BE) was then calculated using the following equation

$$\mathrm{BE} = E_{AB}^{AB} - E_A^{AB} - E_B^{AB}$$

The electrostatic potential (ESP) was calculated using Gaussian 09 [52] at the level of B3LYP/6-311G.

## ASSOCIATED CONTENT

The supporting information can be found on the web and contains: (**Fig. S1**) details for conductance measurements of AZ1, NA1 and AZ2; (**Fig. S2**) DLS analysis of AZ1, AZ2 and NA1; (**Table S1**) averaged particle diameter distribution of AZ1, AZ2 and NA1; (**Table S2**) the conductance values of the studied compounds; (**Fig. S3**) UV-vis absorption spectra measured at different molecular concentrations for AZ1, AZ2 and NA1 in THF/TMB; (**Fig. S4**) control experiments of pure solvent and self-assembled monolayers; (**Fig. S5**) analytical methods for key plateau features and statistics of high conductance states; (**Fig. S6**) the calculated energy profile versus dihedral angles for AZ1 and NA1. (**Fig. S7**) mechanical model of the π-stacked dimer junction; (**Fig. S8**) conductance measurements of 100 μM AZ1+AZ3 mixture and AZ3; (**Fig. S9**) conductance profiles of 'pull and hold' experiments; (**Fig. S10**) calculated energy level diagram of monomers; (**Fig. S11**) transmission functions for monomer AZ1 and NA1; (**Fig. S12**) Binding energy as a function of stretching distance of fully stacked AZ1 dimers and NA1 dimers; (**Fig. S13**) calculated energy level diagram of monomer and dimer AZ1; (**Fig. S14**) calculated energy level diagram of monomer and dimer NA1; (**Fig. S15**) transmission functions for AZ2 monomer and AZ1 monomer; (**Fig. S16**) conductance measurements of DAZS and DAZ; (**Fig. S17**) transmission functions for dimer AZ1 and AZ2; (**Fig. S18**) effect of -SMe rotation on the stacking of AZ1 dimer and AZ2 dimer; (**Fig. S19**) diagram illustrating the relation between influencing factors, π-π stacking and the measured results; (**Table S3** and **Fig. S20**) influence of electric field on twist angle and dipole of AZ1 and NA1; (**Text. S2**) Synthetic procedures; (**Figs. S21-31**) NMR spectra; (**Figs. S32-38**) Mass spectra; (**Figs. S39-49**) infrared spectra; (**Fig. S50**) UV-vis absorption spectra; (**Fig. S51**) Cyclic voltammograms; (**Table S4**) optical and electrochemical data.

## AUTHOR INFORMATION


### Corresponding Author

*jhli@mail.tsinghua.edu.cn
*yueqili@ustc.edu.cn
*c.lambert@lancaster.ac.uk
*gaoxk@mail.sioc.ac.cn

### Author Contributions

# C.Z., J.C. and Q.W. contributed equally to this paper.


### Notes

The authors declare no competing interests.

## ACKNOWLEDGMENT


This work was financially supported by the National Key Research and Development Program of China (No. 2021YFA1200101 and 2021YFA1200104), NSFC (No. 21790362, 22174134 and 22225506) and CAS Project for Young Scientists in Basic Research (YSBR-054). C.J.L. acknowledges financial support from the UK EPSRC, through grant nos. EP/M014452/1, EP/P027156/1 and EP/N03337X/1.


## REFERENCE


1. Deng, J.-H.; Luo, J.; Mao, Y.-L.; Lai, S.; Gong, Y.-N.; Zhong, D.-C.; Lu, T.-B. π-π stacking interactions: Non-negligible forces for stabilizing porous supramolecular frameworks. *Sci. Adv.* **2020**, *6* (2), eaax9976. DOI: 10.1126/sciadv.aax9976.
2. Tuttle, M. R.; Davis, S. T.; Zhang, S. Synergistic Effect of Hydrogen Bonding and π–π Stacking Enables Long Cycle Life in Organic Electrode Materials. *ACS Energy Letters* **2021**, *6* (2), 643-649. DOI: 10.1021/acsenergylett.0c02604.
3. Biswas, S.; Sen, S.; Im, J.; Biswas, S.; Krstic, P.; Ashcroft, B.; Borges, C.; Zhao, Y.; Lindsay, S.; Zhang, P. Universal Readers Based on Hydrogen Bonding or π–π Stacking for Identification of DNA Nucleotides in Electron Tunnel Junctions. *ACS Nano* **2016**, *10* (12), 11304-11316. DOI: 10.1021/acsnano.6b06466.
4. Li, C.; Wu, H.; Zhang, T.; Liang, Y.; Zheng, B.; Xia, J.; Xu, J.; Miao, Q. Functionalized π Stacks of Hexabenzoperylenes as a Platform for Chemical and Biological Sensing. *Chem* **2018**, *4* (6), 1416-1426. DOI: 10.1016/j.chempr.2018.03.007.
5. Wei, X.; Wang, Y.; Xiong, X.; Guo, X.; Zhang, L.; Zhang, X.; Zhou, S. Codelivery of a π–π Stacked Dual Anticancer Drug Combination with Nanocarriers for Overcoming Multidrug Resistance and Tumor Metastasis. *Adv. Funct. Mater.* **2016**, *26* (45), 8266-8280. DOI: 10.1002/adfm.201603336.
6. Wang, X.-Q.; Yang, S.-Y.; Tian, Q.-S.; Zhong, C.; Qu, Y.-K.; Yu, Y.-J.; Jiang, Z.-Q.; Liao, L.-S. Multi-Layer π-Stacked Molecules as Efficient Thermally Activated Delayed Fluorescence Emitters. *Angew. Chem. Int. Ed.* **2021**, *60* (10), 5213-5219. DOI: 10.1002/anie.202011384.
7. Xin, H.; Li, J.; Ge, C.; Yang, X.; Xue, T.; Gao, X. 6,6′ -Diaryl-substituted biazulene diimides for solution-processable high-performance n-type organic semiconductors. *Materials Chemistry Frontiers* **2018**, *2* (5), 975-985. DOI: 10.1039/C8QM00047F.
8. Kim, J. S.; Jung, Y. J.; Park, J. W.; Shaller, A. D.; Wan, W.; Li, A. D. Q. Mechanically Stretching Folded Nano-π-b;-stacks Reveals Pico-Newton Attractive Forces. *Adv. Mater.* **2009**, *21* (7), 786-789. DOI: 10.1002/adma.200801323.
9. Zhang, Y.; Miao, Y.; Song, X.; Gao, Y.; Zhang, Z.; Ye, K.; Wang, Y. Single-Molecule-based White-Light Emissive Organic Solids with Molecular-Packing-Dependent Thermally Activated Delayed Fluorescence. *J. Phys. Chem. Lett.* **2017**, *8* (19), 4808-4813. DOI: 10.1021/acs.jpclett.7b02213.
10. Wu, S.; González, M. T.; Huber, R.; Grunder, S.; Mayor, M.; Schönenberger, C.; Calame, M. Molecular junctions based on aromatic coupling. *Nat. Nanotechnol.* **2008**, *3* (9), 569-574. DOI: 10.1038/nnano.2008.237.
11. Frisenda, R.; Janssen, V. A. E. C.; Grozema, F. C.; van der Zant, H. S. J.; Renaud, N. Mechanically controlled quantum interference in individual π-stacked dimers. *Nat. Chem.* **2016**, *8* (12), 1099-1104. DOI: 10.1038/nchem.2588.
12. Stefani, D.; Weiland, K. J.; Skripnik, M.; Hsu, C.; Perrin, M. L.; Mayor, M.; Pauly, F.; van der Zant, H. S. J. Large Conductance Variations in a Mechanosensitive Single-Molecule Junction. *Nano Lett.* **2018**, *18* (9), 5981-5988. DOI: 10.1021/acs.nanolett.8b02810.
13. Gentil, S.; Serre, D.; Philouze, C.; Holzinger, M.; Thomas, F.; Le Goff, A. Electrocatalytic O2 Reduction at a Bio-inspired Mononuclear Copper Phenolato Complex Immobilized on a Carbon Nanotube Electrode. *Angew. Chem. Int. Ed.* **2016**, *55* (7), 2517-2520. DOI: 10.1002/anie.201509593.
14. Bootsma, A. N.; Doney, A. C.; Wheeler, S. E. Predicting the Strength of Stacking Interactions between Heterocycles and Aromatic Amino Acid Side Chains. *J. Am. Chem. Soc.* **2019**, *141* (28), 11027-11035. DOI: 10.1021/jacs.9b00936.
15. Huber, R. G.; Margreiter, M. A.; Fuchs, J. E.; von Grafenstein, S.; Tautermann, C. S.; Liedl, K. R.; Fox, T. Heteroaromatic π-Stacking Energy Landscapes. *J. Chem. Inf. Model.* **2014**, *54* (5), 1371-1379. DOI: 10.1021/ci500183u.
16. Xiao, Z.-Y.; Zhao, X.; Jiang, X.-K.; Li, Z.-T. Self-assembly of porphyrin–azulene–porphyrin and porphyrin–azulene conjugates. *Org. Biomol. Chem.* **2009**, *7* (12), 2540-2547. DOI: 10.1039/B904009A.
17. Xin, H.; Hou, B.; Gao, X. Azulene-Based π-Functional Materials: Design, Synthesis, and Applications. *Acc. Chem. Res.* **2021**, *54* (7), 1737-1753. DOI: 10.1021/acs.accounts.0c00893.
18. Xu, B.; Tao, N. J. Measurement of Single-Molecule Resistance by Repeated Formation of Molecular Junctions. *Science* **2003**, *301* (5637), 1221. DOI: 10.1126/science.1087481.
19. Zhou, X.-S.; Wei, Y.-M.; Liu, L.; Chen, Z.-B.; Tang, J.; Mao, B.-W. Extending the Capability of STM Break Junction for Conductance Measurement of Atomic-Size Nanowires: An Electrochemical Strategy. *J. Am. Chem. Soc.* **2008**, *130* (40), 13228-13230. DOI: 10.1021/ja8055276.
20. Li, Y.; Buerkle, M.; Li, G.; Rostamian, A.; Wang, H.; Wang, Z.; Bowler, D. R.; Miyazaki, T.; Xiang, L.; Asai, Y.; et al. Gate controlling of quantum interference and direct observation of anti-resonances in single molecule charge transport. *Nat. Mater.* **2019**, *18* (4), 357-363. DOI: 10.1038/s41563-018-0280-5.
21. Yang, W.-Y.; Zheng, J.; Zhang, X.-G.; Chen, L.-C.; Si, Y.; Huang, F.-Z.; Hong, W. Charge transport through a water-assisted hydrogen bond in single-molecule glutathione disulfide junctions. *Journal of Materials Chemistry C* **2020**, *8* (2), 481-486. DOI: 10.1039/C9TC05686F.
22. Park, Y. S.; Whalley, A. C.; Kamenetska, M.; Steigerwald, M. L.; Hybertsen, M. S.; Nuckolls, C.; Venkataraman, L. Contact Chemistry and Single-Molecule Conductance: A Comparison of Phosphines, Methyl Sulfides, and Amines. *J. Am. Chem. Soc.* **2007**, *129* (51), 15768-15769. DOI: 10.1021/ja0773857.
23. Kamenetska, M.; Koentopp, M.; Whalley, A. C.; Park, Y. S.; Steigerwald, M. L.; Nuckolls, C.; Hybertsen, M. S.; Venkataraman, L. Formation and Evolution of Single-Molecule Junctions. *Phys. Rev. Lett.* **2009**, *102* (12), 126803. DOI: 10.1103/PhysRevLett.102.126803.
24. Martín, S.; Grace, I.; Bryce, M. R.; Wang, C.; Jitchati, R.; Batsanov, A. S.; Higgins, S. J.; Lambert, C. J.; Nichols, R. J. Identifying Diversity in Nanoscale Electrical Break Junctions. *J. Am. Chem. Soc.* **2010**, *132* (26), 9157-9164. DOI: 10.1021/ja103327f.
25. Piacenza, M.; Grimme, S. Van der Waals Complexes of Polar Aromatic Molecules: Unexpected Structures for Dimers of

Azulene. *J. Am. Chem. Soc.* **2005**, *127* (42), 14841-14848. DOI: 10.1021/ja053613q.
26. Schwarz, F.; Koch, M.; Kastlunger, G.; Berke, H.; Stadler, R.; Venkatesan, K.; Lörtscher, E. Charge Transport and Conductance Switching of Redox-Active Azulene Derivatives. *Angew. Chem. Int. Ed.* **2016**, *55* (39), 11781-11786. DOI: 10.1002/anie.201605559.
27. Lee, S. A.; Hotta, S.; Nakanishi, F. Spectroscopic Characteristics and Intermolecular Interactions of Thiophene/Phenylene Co-Oligomers in Solutions. *J. Phys. Chem. A* **2000**, *104* (9), 1827-1833. DOI: 10.1021/jp9930604.
28. Zhai, C.; Zhang, P.; Peng, P.; Hou, B.; Li, L. Hydrogen bonding and π-π stacking in nicotinamide/H2O mixtures. *Spectrochim. Acta, Part A* **2017**, *184*, 294-298. DOI: 10.1016/j.saa.2017.05.020.
29. Magyarkuti, A.; Adak, O.; Halbritter, A.; Venkataraman, L. Electronic and mechanical characteristics of stacked dimer molecular junctions. *Nanoscale* **2018**, *10* (7), 3362-3368. DOI: 10.1039/C7NR08354H.
30. Li, X.; Wu, Q.; Bai, J.; Hou, S.; Jiang, W.; Tang, C.; Song, H.; Huang, X.; Zheng, J.; Yang, Y.; et al. Structure-Independent Conductance of Thiophene-Based Single-Stacking Junctions. *Angew. Chem. Int. Ed.* **2020**, *59* (8), 3280-3286. DOI: 10.1002/anie.201913344.
31. Meisner, J. S.; Ahn, S.; Aradhya, S. V.; Krikorian, M.; Parameswaran, R.; Steigerwald, M.; Venkataraman, L.; Nuckolls, C. Importance of Direct Metal−π Coupling in Electronic Transport Through Conjugated Single-Molecule Junctions. *J. Am. Chem. Soc.* **2012**, *134* (50), 20440-20445. DOI: 10.1021/ja308626m.
32. Lv, Y.; Lin, J.; Song, K.; Song, X.; Zang, H.; Zang, Y.; Zhu, D. Single cycloparaphenylene molecule devices: Achieving large conductance modulation via tuning radial π-conjugation. *Sci. Adv.* **2021**, *7* (52), eabk3095. DOI: 10.1126/sciadv.abk3095.
33. Daeffler, K. N. M.; Lester, H. A.; Dougherty, D. A. Functionally Important Aromatic–Aromatic and Sulfur−π Interactions in the D2 Dopamine Receptor. *J. Am. Chem. Soc.* **2012**, *134* (36), 14890-14896. DOI: 10.1021/ja304560x.
34. Yanson, A. I.; Bollinger, G. R.; van den Brom, H. E.; Agraït, N.; van Ruitenbeek, J. M. Formation and manipulation of a metallic wire of single gold atoms. *Nature* **1998**, *395* (6704), 783-785. DOI: 10.1038/27405.
35. Hong, W.; Manrique, D. Z.; Moreno-García, P.; Gulcur, M.; Mishchenko, A.; Lambert, C. J.; Bryce, M. R.; Wandlowski, T. Single Molecular Conductance of Tolanes: Experimental and Theoretical Study on the Junction Evolution Dependent on the Anchoring Group. *J. Am. Chem. Soc.* **2012**, *134* (4), 2292-2304. DOI: 10.1021/ja209844r.
36. Tang, Y.; Zhou, Y.; Zhou, D.; Chen, Y.; Xiao, Z.; Shi, J.; Liu, J.; Hong, W. Electric Field-Induced Assembly in Single-Stacking Terphenyl Junctions. *J. Am. Chem. Soc.* **2020**, *142* (45), 19101-19109. DOI: 10.1021/jacs.0c07348.
37. Yu, H.; Li, J.; Li, S.; Liu, Y.; Jackson, N. E.; Moore, J. S.; Schroeder, C. M. Efficient Intermolecular Charge Transport in π-Stacked Pyridinium Dimers Using Cucurbit[8]uril Supramolecular Complexes. *J. Am. Chem. Soc.* **2022**, *144* (7), 3162-3173. DOI: 10.1021/jacs.1c12741.
38. Venkataraman, L.; Klare, J. E.; Nuckolls, C.; Hybertsen, M. S.; Steigerwald, M. L. Dependence of single-molecule junction conductance on molecular conformation. *Nature* **2006**, *442* (7105), 904-907. DOI: 10.1038/nature05037.
39. Vonlanthen, D.; Mishchenko, A.; Elbing, M.; Neuburger, M.; Wandlowski, T.; Mayor, M. Chemically Controlled Conductivity: Torsion-Angle Dependence in a Single-Molecule Biphenyldithiol Junction. *Angew. Chem. Int. Ed.* **2009**, *48* (47), 8886-8890. DOI: 10.1002/anie.200903946.
40. Wang, H.; Wang, Z.; Wang, Y.; Hihath, J.; Chen, H.-Y.; Li, Y.; Tao, N. Potential Dependence of Mechanical Stability and Electronic Coupling of Single S–Au Bonds. *J. Am. Chem. Soc.* **2018**, *140* (51), 18074-18081. DOI: 10.1021/jacs.8b10857.
41. Büttiker, M.; Imry, Y.; Landauer, R.; Pinhas, S. Generalized many-channel conductance formula with application to small rings. *Phys. Rev. B* **1985**, *31* (10), 6207-6215. DOI: 10.1103/PhysRevB.31.6207.
42. Nitzan, A. ELECTRON TRANSMISSION THROUGH MOLECULES AND MOLECULAR INTERFACES. *Annu. Rev. Phys. Chem.* **2001**, *52* (1), 681-750. DOI: 10.1146/annurev.physchem.52.1.681.
43. Akkerman, H. B.; de Boer, B. Electrical conduction through single molecules and self-assembled monolayers. *J. Phys-Condens. Mat.* **2007**, *20* (1), 013001. DOI: 10.1088/0953-8984/20/01/013001.
44. Adak, O.; Rosenthal, E.; Meisner, J.; Andrade, E.; Pasupathy, A.; Nuckolls, C.; Hybertsen, M.; Venkataraman, L. Flicker Noise as a Probe of Electronic Interaction at Metal–Single Molecule Interfaces. *Nano Lett.* **2015**, *15*. DOI: 10.1021/acs.nanolett.5b01270.
45. Tang, C.; Huang, L.; Sangtarash, S.; Noori, M.; Sadeghi, H.; Xia, H.; Hong, W. Reversible Switching between Destructive and Constructive Quantum Interference Using Atomically Precise Chemical Gating of Single-Molecule Junctions. *J. Am. Chem. Soc.* **2021**, *143* (25), 9385-9392. DOI: 10.1021/jacs.1c00928.
46. Chen, H.; Zheng, H.; Hu, C.; Cai, K.; Jiao, Y.; Zhang, L.; Jiang, F.; Roy, I.; Qiu, Y.; Shen, D.; et al. Giant Conductance Enhancement of Intramolecular Circuits through Interchannel Gating. *Matter* **2020**, *2* (2), 378-389. DOI: 10.1016/j.matt.2019.12.015.
47. Zhu, Z.; Qu, H.; Chen, Y.; Zhang, C.; Li, R.; Zhao, Y.; Zhou, Y.; Chen, Z.; Liu, J.; Xiao, Z.; et al. Single-molecule conductance variations of up to four orders of magnitude via contacting electrodes with different anchoring sites. *Journal of Materials Chemistry C* **2021**, *9* (45), 16192-16198. DOI: 10.1039/D1TC03506A.
48. Tang, C.; Chen, L.; Zhang, L.; Chen, Z.; Li, G.; Yan, Z.; Lin, L.; Liu, J.; Huang, L.; Ye, Y.; et al. Multicenter-Bond-Based Quantum Interference in Charge Transport Through Single-Molecule Carborane Junctions. *Angew. Chem. Int. Ed.* **2019**, *58* (31), 10601-10605. DOI: 10.1002/anie.201904521.
49. Garner, M. H.; Li, H.; Chen, Y.; Su, T. A.; Shangguan, Z.; Paley, D. W.; Liu, T.; Ng, F.; Li, H.; Xiao, S.; et al. Comprehensive suppression of single-molecule conductance using destructive σ-interference. *Nature* **2018**, *558* (7710), 415-419. DOI: 10.1038/s41586-018-0197-9.
50. W.H., K. Van der Waals attractive force. *Phys. Z.* **1921**, *22*, 129–141.
51. Soler, J. M.; Artacho, E.; Gale, J. D.; García, A.; Junquera, J.; Ordejón, P.; Sánchez-Portal, D. The SIESTA method forab initioorder-Nmaterials simulation. *J. Phys-Condens. Mat.* **2002**, *14* (11), 2745-2779. DOI: 10.1088/0953-8984/14/11/302.
52. M.J. Frisch, G. W. T., H.B. Schlegel, G.E. Scuseria, M.A. Robb, J.R. Cheeseman, G. Scalmani, V. Barone, G.A. Petersson, H. Nakatsuji, X. Li, M. Caricato, A.V. Marenich, J. Bloino, B.G. Janesko, R. Gomperts, B. Mennucci, H.P. Hratchian, J.V. Ortiz, A.F. Izmaylov, J.L. Sonnenberg, D. Williams-Young, F. Ding, F. Lipparini, F. Egidi, J. Goings, B. Peng, A. Petrone, T. Henderson, D. Ranasinghe, V.G. Zakrzewski, J. Gao, N. Rega, G. Zheng, W. Liang, M. Hada, M. Ehara, K. Toyota, R. Fukuda, J. Hasegawa, M. Ishida, T. Nakajima, Y. Honda, O. Kitao, H. Nakai, T. Vreven, K. Throssell, J.A. Montgomery Jr., J.E. Peralta, F. Ogliaro, M.J. Bearpark, J.J. Heyd, E.N. Brothers, K.N. Kudin, V.N. Staroverov, T.A. Keith, R. Kobayashi, J. Normand, K. Raghavachari, A.P. Rendell, J.C. Burant, S.S. Iyengar, J. Tomasi, M. Cossi, J.M. Millam, M. Klene, C. Adamo, R. Cammi, J.W. Ochterski, R.L. Martin, K. Morokuma, O. Farkas, J.B. Foresman, D.J. Fox. Gaussian 16; Gaussian, Inc., Wallingford, CT (2016).
53. Ferrer, J.; Lambert, C. J.; García-Suárez, V. M.; Manrique, D. Z.; Visontai, D.; Oroszlany, L.; Rodríguez-Ferradás, R.; Grace, I.; Bailey, S. W. D.; Gillemot, K.; et al. GOLLUM: a next-generation

simulation tool for electron, thermal and spin transport. *New J. Phys.* **2014**, *16* (9), 093029. DOI: 10.1088/1367-2630/16/9/093029.
54. Valeev, E. F.; Coropceanu, V.; da Silva Filho, D. A.; Salman, S.; Brédas, J.-L. Effect of Electronic Polarization on Charge-Transport Parameters in Molecular Organic Semiconductors. *J. Am. Chem. Soc.* **2006**, *128* (30), 9882-9886. DOI: 10.1021/ja061827h.
55. Zhou, Y.; Long, G.; Li, A.; Gray-Weale, A.; Chen, Y.; Yan, T. Towards predicting the power conversion efficiencies of organic solar cells from donor and acceptor molecule structures. *Journal of Materials Chemistry C* **2018**, *6* (13), 3276-3287. DOI: 10.1039/C7TC05290A.
56. Mansø, M.; Koole, M.; Mulder, M.; Olavarria-Contreras, I. J.; Andersen, C. L.; Jevric, M.; Broman, S. L.; Kadziola, A.; Hammerich, O.; van der Zant, H. S. J.; et al. Synthesis and Single-Molecule Conductances of Neutral and Cationic Indenofluorene-Extended Tetrathiafulvalenes: Kondo Effect Molecules. *J. Org. Chem.* **2016**, *81* (18), 8406-8414. DOI: 10.1021/acs.joc.6b01579.
57. Zhang, Z.; Miao, J.; Ding, Z.; Kan, B.; Lin, B.; Wan, X.; Ma, W.; Chen, Y.; Long, X.; Dou, C.; et al. Efficient and thermally stable organic solar cells based on small molecule donor and polymer acceptor. *Nat. Commun.* **2019**, *10* (1), 3271. DOI: 10.1038/s41467-019-10984-6.
58. Pommerehne, J.; Vestweber, H.; Guss, W.; Mahrt, R. F.; Bässler, H.; Porsch, M.; Daub, J. Efficient two layer leds on a polymer blend basis. *Adv. Mater.* **1995**, *7* (6), 551-554. DOI: 10.1002/adma.19950070608.
59. Cheng, Z. L.; Skouta, R.; Vazquez, H.; Widawsky, J. R.; Schneebeli, S.; Chen, W.; Hybertsen, M. S.; Breslow, R.; Venkataraman, L. In situ formation of highly conducting covalent Au–C contacts for single-molecule junctions. *Nat. Nanotechnol.* **2011**, *6* (6), 353-357. DOI: 10.1038/nnano.2011.66.
60. Li, Y.; Xiang, L.; Palma, J. L.; Asai, Y.; Tao, N. Thermoelectric effect and its dependence on molecular length and sequence in single DNA molecules. *Nat. Commun.* **2016**, *7* (1), 11294. DOI: 10.1038/ncomms11294.

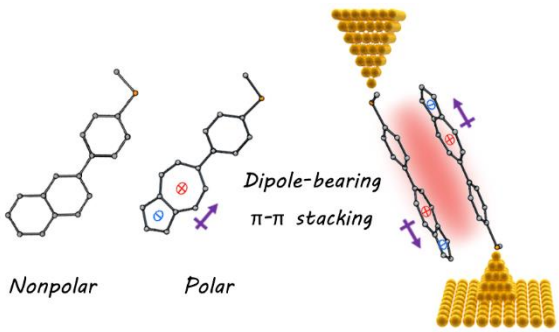
Dipole-bearing
π-π stacking
Nonpolar
Polar